Chapter 16
Neural Interfacing with the Peripheral Nervous System: A FINE Approach

Dominique M. Durand, Brian Wodlinger, and HyunJoo Park

1 Neurotechnology for Interfacing with the Peripheral Nervous System

Functional Electrical Stimulation (FES) strives to restore function to neurologically impaired individuals by electrically activating intact tissue distal to a neural lesion. Until recently, clinical neuromuscular control has been achieved by placing electrodes in or on the muscle, near the motor point. There are, however, several disadvantages to these systems that limit the potential for future advances. The stimulation current requirements for intramuscular (IM) electrodes are one to two orders of magnitude higher than those necessary to stimulate the axon directly. Also, with IM systems, at least one electrode must be implanted per muscle, requiring multiple involved surgical procedures and an unacceptable number of leads to service and maintain. Mechanical failure of the electrodes frequently arises from the stress generated by contracting muscles. Further, the recruitment properties of the electrodes are neither stable nor reliable. As the muscle contracts, the stimulation site moves relative to the muscle motor point and generates a recruitment curve dependent upon muscle length. In addition, electrode migration causes varying recruitment characteristics over time and stimulation spillover to unwanted muscles. Consequently, many researchers have been searching for methods to directly stimulate the efferent motor neurons in peripheral nerves.

D.M. Durand (✉) • H. Park
Department of Biomedical Engineering, Neural Engineering Center,
Case Western Reserve University, Cleveland, OH 44106, USA
e-mail: dxd6@case.edu

B. Wodlinger
Department of Biomedical Engineering, Neural Engineering Center,
Case Western Reserve University, Cleveland, OH 44106, USA

Department of Physical Medicine & Rehabilitation, University of Pittsburgh,
Pittsburgh, PA, USA

Direct nerve stimulation offers many advantages over IM stimulation. It is possible to control many muscles with one electrode array, so that only a single implant procedure is required. The neural electrodes can also be implanted in locations with relatively little motion and stress. Hence, they are less susceptible to mechanical failure and do not exhibit length-dependent recruitment properties. Furthermore, the stimulation currents are one to two orders of magnitude lower than those of the muscle electrodes and require much less power to provide muscle function. A highly selective electrode could stimulate separate motor units sequentially, allowing fine motor control with reduced muscle fatigue. Finally, nerve electrodes have the potential to record afferent signals, and show promise as a means of supplying feedback for neuromuscular control.

1.1   Interface Systems with Peripheral Nerves

Modern neural electrodes are used for both stimulation and recording, and can be classified as extraneural (round or flat interface) and endoneural (intrafascicular). This distinction is based upon the neural membranes (epineurium or perineurium) that are disrupted by the electrodes. The different properties and functions of these membranes make this classification important. The epineurium is a soft, loose connective tissue whose main purpose is to bind the fascicles together [1]. The perineurium, on the other hand, is a tough membrane several cell layers thick that serves multiple functions: regulating endoneurial solute concentrations, maintaining positive intrafascicular pressure, and serving as a barrier to infection. Electrodes that pierce the perineurium are more likely to damage the nerve than those that do not.

Round extraneural electrodes pierce neither membrane, reshape the nerve into a round shape or use multiple contacts placed around the nerve for selective stimulation and recording. These electrodes can cause some damage but it appears to be reversible [2]. They are limited in stimulation and recording selectivity because some fascicles are located in the center of the nerve away from the electrodes. Modeling and experimental studies have demonstrated that round extraneural electrodes tend to recruit motor units in "inverse order," and recruit small fascicles before large fascicles [3]. Moreover, it is difficult to access deep regions of the nerve without stimulating surface regions [4–6]. Different stimulation protocols have been tried with mixed success to correct these problems, including tripole electrode configurations [7, 8], "pre-pulsing" [9], and steering currents [7, 8, 10]. Current round extraneural electrode designs include the spiral [11–14], and the helix [15]. The spiral and helix electrodes have self-sizing properties to allow for neural swelling and inflammation, while providing a tight coupling between the nerve and electrical contacts. The spiral and cuff-type electrodes provide an insulating surface around the nerve that lowers stimulation thresholds by confining current to the nerve.

Whole nerve recording has also been performed with extraneural cuff electrodes. In humans, the sural nerve has been used to provide sensory feedback for correction of foot-drop [16]. Also, slip control in hand-grasp has been aided with recording from the radial branch of a digital palmar nerve [17]. Spiral cuffs implanted on the hypoglossal nerves of anesthetized cats were able to monitor the animal's respiratory drive, and stable recordings have been obtained from the hypoglossal nerve of a dog over a 14-month period [18]. There have also been efforts to localize ENG signals within the nerve using multi-contact electrodes, and recent experiments have demonstrated limited fascicle level selectivity under specialized conditions. Experiments carried out in rabbits used oval cuffs to account for the normal, flat geometry of the sciatic nerve [19], and showed a modest ability to discriminate between two fascicles at opposite sides of the nerve. Higher levels of selectivity with cuff electrodes have been reported [20–22].

1.2 Intrafascicular Nerve Electrodes

Intrafascicular electrodes penetrate both neural membranes and can provide selective activation of small subsets of axons and more information from sensory afferents than extraneural electrodes. Models have also shown a more physiologic recruitment pattern for intrafascicular electrodes. Unfortunately, they can damage the axons and require delicate implant procedures, and some designs are not applicable for chronic implantation. There are four types of intrafascicular electrodes: the regeneration arrays, multiple electrode arrays (Utah array), the longitudinal intrafascicular electrode (LIFE), and the transverse intrafascicular electrode (TIME). The regeneration array [23, 24] is a perforated silicon plane with a metal electrode sputtered around each hole for stimulation and recording. This electrode is sutured between two ends of a severed nerve, and, in theory, the axons regenerate through the holes. If the holes are very small, the axons will be unable to penetrate and tend to regenerate around the array. This design is obviously damaging as the nerve must be completely severed. However, it can provide useful information for short periods [25]. Micromachined silicon probes have also been used for intrafascicular stimulation and recording. Three-dimensional multi-contact electrodes [26, 27] have been fabricated. The stimulation selectivity for the Utah slanted array is quite high [28]. This electrode pierces the perineurium at several points. Although viable axons are seen next to the electrodes, this array can cause significant disruption in the cross section of the nerve. The recorded sensory signals were not always stable. The LIFE interface consists of very thin electrical wires (up to 24) or thin substructure with electrical contacts threaded into the fascicles. Single unit recording resolution [29], as well as stimulation selectivity, has been achieved [30–32]. Muscle fatigue has been reduced using interleaved stimulation with two wire electrodes in the same fascicle [33]. This electrode has also been used for stimulation and recording in human amputees [34, 35]. Significant tissue reaction, edema, and scarring are evident at the point of wire entry into the fascicle [36].

The TIME interface is a more recent development whereby a cable with multiple contacts is inserted within the nerve transversely and allows contacts within the cable to record or stimulate the nerve [37].

These intrafascicular electrodes have significant advantages as they provide intimate contacts with the neural tissue and can generate high degrees of selectivity for stimulation and high signal-to-noise ratios for recordings. However, there are also significant questions concerning the long-term stability of recruitment and recording properties due to the movement of the probe tip relative to the axons. Moreover, these electrodes penetrate the perineurium, a highly protective membrane, and could cause significant damage.

1.3   Flat Interface Nerve Electrode

The flat interface electrode design was recently introduced [38]. This design takes advantage of the fact that nerves are not round but rather oblong in shape and that the nerve shape is plastic. Recent observations suggest that the cross-sectional geometries of nerve trunks are generally ellipsoid in shape and these geometries are created by the local anatomy of the surrounding tissue [39]. Experimental data also show that nerve cross-sectional geometries can also be reshaped by extraneural electrodes [40]. Extraneural electrodes such as the spiral [11, 41] and the helix [42] have cylindrical cross sections and actually reshape the nerve into a round configuration. Some nerves or portions of nerves have an already nearly flat configuration such as the human femoral nerve shown in Fig. 16.1. Other nerves such as the hypoglossal nerve and pudendal nerve are nearly flat in some sections. Since the round shape minimizes the ratio of circumference to cross-sectional area, it is the shape that provides the least amount of space to place the electrodes. Conversely, the flat shape will allow a much higher electrode density.

To improve the selectivity of extraneural nerve electrodes, the flat interface nerve electrode (FINE) [38] was designed, built, and tested. The FINE is designed to either maintain a nerve in its original flat configuration or to reorganize the transverse cross section of the nerve and its fascicles into ovals by applying a small, non-circumferential force to the nerve.

Computer simulations [43] and experiments have shown that by realigning the fascicles within the electrode, the FINE provides both fascicular [38] and subfascicular [44] selectivities. Stimulation selectivity has been demonstrated in acute and chronic experiments, in the sciatic and the hypoglossal nerve. A chronic study of this electrode has shown that simply aligning the fascicle is safe while reshaping the fascicles drastically can cause transient damage [45]. The electrode has now been implanted in human patients safely for short period of time [46].

One of the most challenging problems in peripheral nerve stimulation is the fact that the conventional electrode configurations always recruit larger motor units before smaller ones [47] contrary to the physiological recruitment order. Nerve diameter selective stimulation is important in restoring some motor functions, e.g.,
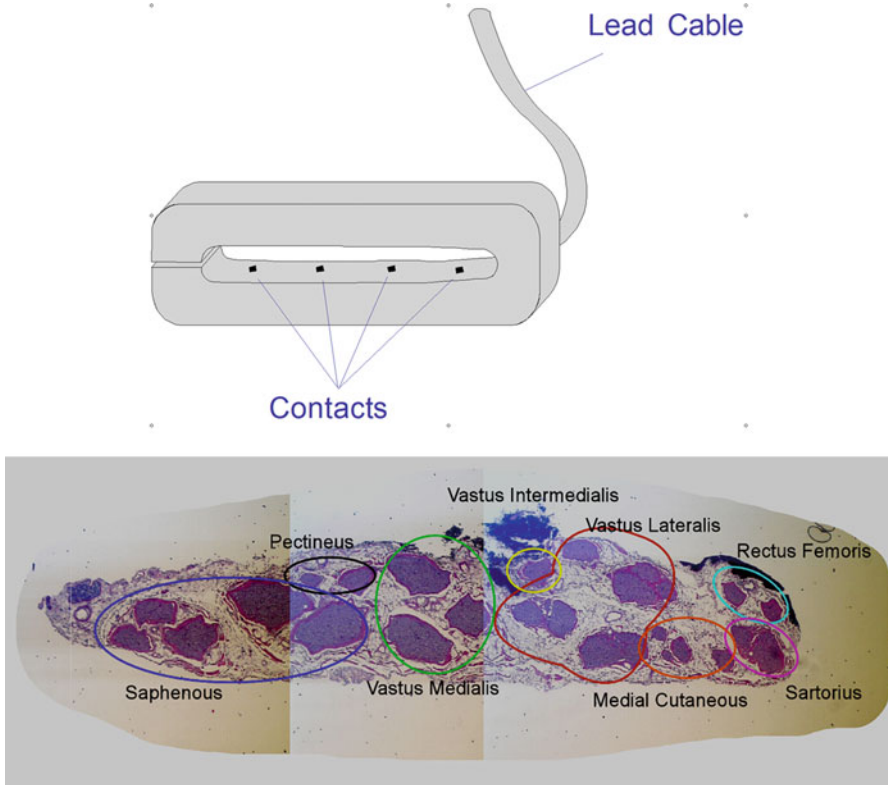
Fig. 16.1 (**a**) Silicone implementation of the FINE used for rats experiments. Opening height of the electrode is 0.4 mm. (**b**) Cross section of a human femoral nerve indicating the natural flat shape

the functional movement [48, 49] and bladder prosthesis [50, 51]. Several stimulation techniques have been proposed to solve this problem; anodic block [50–54], single cathode [55], and subthreshold-depolarizing prepulse [56–58]. These techniques rely on the properties of sodium channels and require a long-duration stimulating pulse (>500 μs), which could lead to electrode corrosion [59].

However, previous studies have showed that excitability of axons within specific diameter range could be controlled by manipulating the extracellular voltage profile (V_e) along the nerve fiber [60]. The technique relies on the fact that excitability of myelinated axons is reciprocal to the second spatial difference of V_e and that the internodal distance of myelinated axons is proportional to the axon diameter. Results from computer simulations and animal experiments show that an array of alternating four cathodes and five anodes with 1.2 mm intercathodic distance could suppress the excitability of axons having diameter within the 12 ± 2 μm range, and that the technique was independent of stimulating pulse width [61].

Selective recording from nerves is another difficult problem. For most individuals with SCI and stroke survivors, a significant portion of the peripheral nervous system is intact and can provide viable sources for FES control signals. As such, recording the electrical activity from a whole nerve or functionally specific branches is a particularly appealing choice. Unlike recording methods associated with EMG or EEG, direct neural recordings are specific and provide rapid feedback. In addition to the relatively noninvasive surgical procedure associated with nerve cuff electrodes, the reported long-term reliability and safety of these devices offer further validation for the implementation of this technology into FES systems [62]. The majority of FES applications involve nerve trunks (e.g., radial, sciatic or hypoglossal nerves) that consist of multiple bundles of motor and sensory fibers, the electrical activity of which could be used to control both the *afferent* and *efferent* pathways involved with the prosthesis. As a consequence, multi-contact cuff electrodes have been developed to circumvent the need for multiple electrodes implanted on each distal nerve branch. While numerous studies have documented the selective stimulation properties of these conventionally round (i.e., transverse geometry) and even self-sizing electrodes [11], there is a paucity of experimental data concerning the ability of such electrodes to record and distinguish between different active fascicles [21, 22].

FINE presents a unique cuff design for selective nerve recording by realigning the fascicles and reshaping the nerve into a more flattened cross section. Several studies have been aimed at determining the safety of the electrodes in animal chronic implants [45, 63]. In particular, the pressure generated by the electrode was estimated and the electrodes are designed to minimize the pressure and allow the neural tissue to be reshaped and not compressed since the cross section of the electrode is greater than that of the nerve. Moreover, the electrode height is kept greater than that of the largest fascicle. This electrode has now been shown to be safe, has been approved by the FDA for short duration human implants and has been tested in humans for selective stimulation [46]. One goal of selective stimulation is to restore sensation in patients with limb amputation. In the remainder of the chapter, we provide recent information on the problem of obtaining voluntary signals from nerves of amputees to control artificial limbs.

2   Selective Recording of Peripheral Neural Activity

Physiological sensors function on a number of timescales and through a large variety of mechanisms. While it may be possible to sense these physiological variables as accurately using artificial means, creating sensors with sufficient long-term biocompatibility and cosmesis is extremely difficult. Recording from peripheral nerves presents the opportunity to recover not only the signals of a wide variety of physiological sensors, but also physiological command signals controlling the functions of muscles and other organs. Even though this technology presents a variety of opportunities, it also presents several challenges. This section

discusses the problem of how to separate the mixed signals of interest in a peripheral nerve recording.

Attempts to address the mixing of biological signals have been made for a number of approaches. For example spatial filtering has become quite common in EEG recordings in order to minimize the levels of cross-talk [64]. Only recently has this issue attained significance in the peripheral nervous systems. Zariffa and Popovic [65] have implemented several approaches to solve the inverse problem in nerve cuff recordings, reconstructing individual neural sources from the mixed data recorded on the surface of the nerve. Tesfayesus and Durand [66] recently applied blind source separation (BSS) to perform similar de-mixing of the recorded signals, without the need for a model of the nerve geometry. These techniques will be discussed below with particular emphasis to those presented in Wodlinger and Durand [67] as they been have investigated thoroughly in both simulation and animal models.

2.1 Detection Algorithms

Signal separation algorithms fall into two main categories: BSS, and Inverse Problems (IP) including Beamforming/Spatial Filtering (BF). These techniques are reviewed below. The classic inverse problem solutions with regularization are treated separately from the beamforming method.

2.2 Blind Source Separation

When working with biological systems, especially those of unknown or constantly changing geometry such as nerves, a more robust technique is needed. BSS uses statistical information in the recordings to automatically de-mix the neural signals. This technique makes two important assumptions: the first is that the neural signals are mixed linearly, an assumption supported by Maxwell's equations of the quasi-static propagation of current in the volume conductor. The second assumption is that the neural signals are statistically independent, such that maximizing the statistical independence of linear combinations of the recordings can reproduce them. This assumption is less clear and may depend on the nature of the training data available and the relationship between the signals of interest.

BSS algorithms also introduce a permutation ambiguity, where sources can appear swapped between successive time windows. This ambiguity can be readily solved using techniques presented in Tesfayesus and Durand [66], who demonstrate the benefits of BSS techniques to nerve cuff recordings.

2.3 Classic Inverse Problem Solutions (IP)

Inverse problem algorithms are based on the idea that a rigorous and complete forward model of the system can be found. This model can then be inverted so that for a given output one can calculate a (usually infinite) set of likely inputs. Regularization can be applied to improve the stability of the inversion, or apply additional constraints on the system to help identify the most useful possible inputs. This family of techniques can be extremely powerful when good models are available, and has been used successfully in magnetoencephalography (MEG)-based source localization [68], mapping epicardial potentials from chest surface recordings, and impedance spectroscopy [69] and EEG source imaging [70]. As a matrix inversion is required, the results can be slow and sensitive to model inaccuracy or choice of regularization parameter.

2.4 Spatial Filtering or Beamforming

Spatial filtering, or Beamforming, presents a compromise between techniques requiring extensive accurate models and those requiring none. Rather than trying to explicitly invert the given model, these techniques calculate a set of (usually linear) filters which can be applied to new data to estimate source levels. Spatial filtering methods are particularly well suited to nerve cuffs because of the spatial separation between functional (fascicular) sources, and small internal area of the cuff.

Filters can be calculated using a number of methods, from simple Laplacian operators used to take the second spatial difference to methods requiring the sensitivity fields of each contact on the electrode. These techniques are generally very fast after training, requiring a simple matrix multiplication at each time step. However, they suffer from poor performance compared to IP algorithms, and so they are often combined with a post-processing stage to improve performance. This post-processing is usually adaptive in nature, for example the large array of techniques presented in Sekihara and Nagarajan [71].

A variation of a beamforming technique is presented in the following sections, and in more details in Wodlinger and Durand [72]. This beamforming filter is calculated using an FEM model of the nerve cuff in saline, and includes a static (i.e., non-adaptive) post-processing technique to improve separation quality without requiring statistical independence of the signals. Results are presented to demonstrate the performance of the system on simulated and animal model data.

2.4.1 Beamforming Algorithm Mapping

A computer model of a flat interface peripheral nerve electrode (FINE) placed on a homogenous nerve model is shown in Fig. 16.2a, b. This Finite Element Model
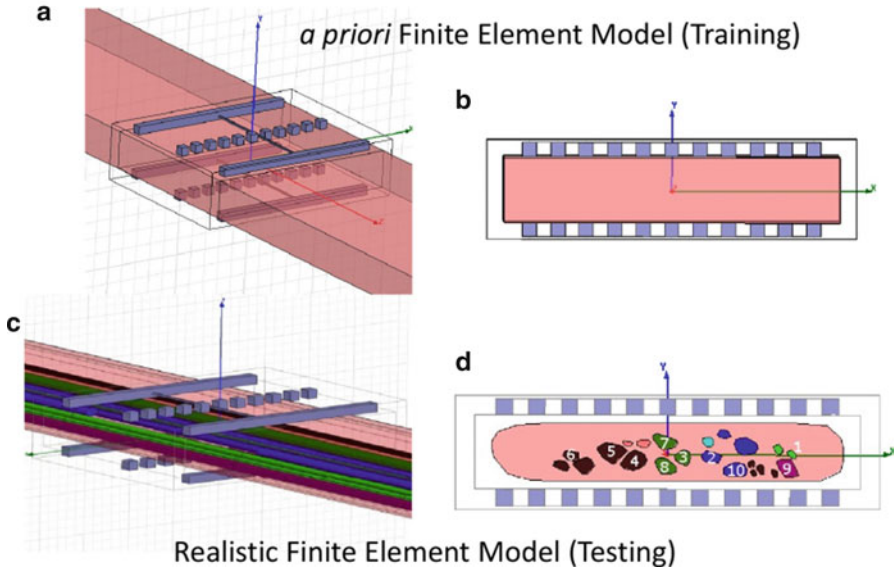
Fig. 16.2 Finite element models generated to test and train the beamforming algorithm. Parts (**a**) and (**b**) show isometric and cross-sectional views (respectively) of the a priori model (apFEM) containing an insulating cuff with 22 contacts (in addition to upper and lower tripoles) and a simple rectangular epineurium filling the cuff. This model was used to generate the spatial filters, or beamformers, for the transformation matrix. Parts (**c**) and (**d**) show isometric and cross-sectional views (respectively) of the realistic model (rFEM), which contains the same cuff but with anisotropic endoneuria, and perineuria around each of the 22 fascicles. Fascicles used in testing are *numbered* and *color-coded* to correspond to the functional group. The geometry for this model is obtained from realistic cross sections of the human femoral nerve presented in Schiefer et al. [73]. Figure reproduced from Wodlinger and Durand [67] with permission from IEEE-TNSRE

(FEM) may be used to calculate the lead-field matrix, or forward problem, which relates the voltage recorded on each contact to the source current at each voxel within the nerve. This simple homogeneous nerve model represents our pre-implantation knowledge of the geometry (the a priori FEM, or apFEM) and provides the necessary information to calculate the beamforming or spatial filters. A more realistic model (the realistic FEM or rFEM) used to test the resulting filters is shown in Fig. 16.2c, d.

2.4.2 Beamforming Filter Matrix

To calculate the Beamforming Filter Matrix, the weights (t_i) on the sensitivity vectors (S) for each contact are optimized for a source signal located in a single ideal pixel (δ_i). Equation (16.1) is solved for each pixel i where

$$St_i = \delta_i. \tag{16.1}$$

Assuming n recording contacts and m pixels in the desired reconstruction, the variables are $S^{\{m \times n\}}$, the sensitivity matrix, and $t_i^{\{n \times 1\}}$ the linear coefficients of the Beamforming Filter Matrix. Note that this equation is entirely independent of time and considers only the static behavior of the model. For increased efficiency, the reduced QR factorization of $S^{\{m \times n\}}$ is first calculated so that for δ_i equal to the delta function at index i, the solution reduces to Eq. (16.2), where q_i^* is the ith row of Q (since Q is orthogonal, the transpose acts as an inverse on the range). Normalization is performed for each set of weights, as in Eq. (16.3).

$$t_i = R/q_i^*, \tag{16.2}$$

$$t_i = \frac{t_i}{\|St_i\|}. \tag{16.3}$$

The column vectors t_i can then be concatenated to form the Beamforming filter matrix $T^{\{m \times n\}}$, which operates on a single time point t of observed data ($o^{\{n \times 1\}}$) to produce the estimated activity at each pixel ($\hat{a}^{\{m \times 1\}}$) at time t, as in Eq. (16.4). This activity vector can then be displayed as an image of the estimated activity in the plane of interest. Repeated application of the Beamforming filter matrix at different time points gives time dependence to this procedure:

$$\hat{a} = To. \tag{16.4}$$

2.4.3 Source Localization

When the Beamforming filter matrix is multiplied by the vector of voltages on each contact [Eq. (16.4)], an image is created providing an estimate of the activation of each pixel within the cross section of the nerve. A simple local-maxima-based algorithm was used to locate sources in the estimate using automatic thresholding to remove areas of low activity [74]. Morphological opening (erosion followed by dilation), which removes islands and peninsulas below a given size from a binary image, was applied to prevent the algorithm from finding small sources near the periphery associated with noise. Once the fascicle locations are determined, the beamformers for those locations are applied to the full time-signal in order to reconstruct the fascicular activity. Post-processing techniques, such as RMS windowed averaging or BSS, can improve SNR and reduce cross-talk.

2.4.4 Source-Based Filter Generation

Filters for a given real neural source may be calculated by averaging the columns of T over which the activity is observed. To improve the determination of the spatial extent of the sources, new filters are generated to take into account information

from other locations. The filters from each pixel are weighted by the value of the source image at that pixel and averaged. This method places more emphasis on locations where the source is stronger, and provides some spatial averaging to reduce noise.

$$f_i = S_i^T M, \tag{16.5}$$

where n is the number of contacts, m the number of pixels, $f_i^{\{1 \times n\}}$ the filter for the ith source, $S_i^{\{m \times 1\}}$ the source image for that source, and $M^{\{m \times n\}}$ is the Beamforming Filter Matrix. In order to reduce sensitivity to areas with high interference, the spatial locations causing interference are iteratively subtracted from each filter using the following:

1. Calculate the interference (I_{ij}) due to source j picked up by the filter for source i

$$I_{ij} = (Mf_i^T)^T S_j | i \neq j \tag{16.6}$$

2. Subtract or add the difference between the images, multiplied by the amount of incorrect signal in each to reduce the amount of interfering signal

$$S_i = S_i - \sum_{(j|j=i)} I_{ij}(S_j - S_i) \tag{16.7}$$

3. Repeat, also recalculating the filters as in Eq. (16.5), until threshold is reached, or previous iteration was ineffective at removing inference

2.5   Signal Separation in Computer Models

To form an accurate model of recorded neural activity, a volume conductor FEM was combined with template models of action potentials as in Jezernik and Sinkjaer [75], Yoo and Durand [76], and Tesfayesus et al. [77]. These templates are randomly delayed and summed to create a simulated ENG signal with the desired temporal characteristics.

2.5.1   Localization of Sources

In order to examine the localization capability of the beamforming filters, a simulated signal isolated to a particular fascicle was created as described above (Fig. 16.3a). The signal power (RMS) at each contact was calculated in 10 ms bins, and the beamforming localization procedure was applied to each (Fig. 16.3b) and the mean of the resulting list of sources was calculated. This estimated location (green cross, Fig. 16.3c) was then compared to the known location
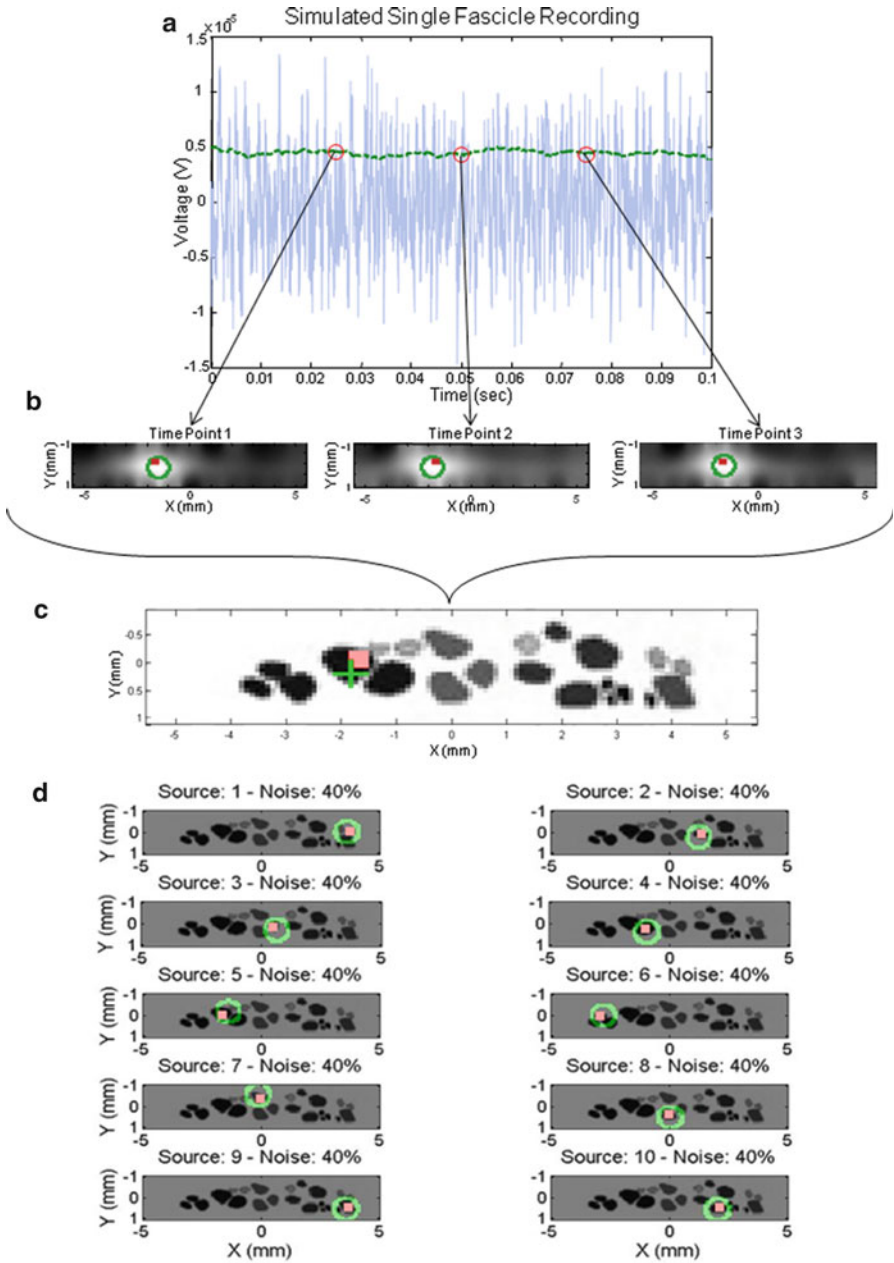
Fig. 16.3 Localization using realistic signals. (**a**) Sample signal of single fascicle activity recorded on a single contact. The signal power (RMS) is shown as a *dark thick line*, while the raw signal is *light* and *thin*. (**b**) Localization results for each of the three marked time points in (**a**). The estimated location is marked with a *green circle*, and the actual location with a *red square*. (**c**) To locate the source, the mean location of all reconstructions is used. This final localization

(red square, Fig. 16.3c) and overlaid onto the fascicle map of the nerve for reference. This process was repeated and the results for one trial of all 10 fascicles at 40% noise are shown in Fig. 16.3d, where the estimated source is shown as a green circle and the true location as a red square. Even at this noise level, the figure clearly shows that all 10 sources are located within their respective fascicles.

In noise-free signals, sources could be located within 0.14 ± 0.03 mm ($N = 100$) of their fascicle's center. As the noise level was increased to 40%, the mean and standard deviation both increase to 0.18 ± 0.17 mm ($N = 100$). These results suggest that the location of single sources can be identified to 180 ± 170 µm even in the presence of significant noise in the signal.

2.5.2 Recovery of Two Active Sources

To demonstrate the ability of the beamforming algorithm to resolve two mixed signals, simulated single fascicle recordings (SR) were summed, two at a time with 0, 10 or 40% added Gaussian noise. The beamforming algorithm was applied at each time point and the pixels corresponding to each fascicle's center were used to generate the Reconstructed Fascicle 1 (RF1) and Reconstructed Fascicle 2 (RF2) signals. The correlation of the reconstructed signals to the original inputs (SR with RF) was calculated after applying a 10-ms RMS windowed average to improve noise tolerance. The process was repeated 10 times for each pair of fascicles with new signals randomly generated each time.

An example of the RMS averaged actual and recovered signals is shown in Fig. 16.4a. These signals show very low cross-talk and each pair is highly correlated ($R > 0.9$). The correlation coefficients for all fascicle pairs are plotted versus the distance between the fascicle centers in Fig. 16.4b. The figure shows R increasing towards 1 with larger separation distance, as expected since less mixing occurs between sources that are further apart. Recovery with $R > 0.9$ was achieved for sources separated by a minimum distance of approximately 1.5 mm.

2.5.3 Effect of Multiple Active Fascicles

In a physiological situation, there would likely be more than two fascicles from which to record (depending on the nerve and location). Therefore, we tested the ability of the algorithm to recover signals from n simultaneously active fascicles,

---

Fig. 16.3 (continued) result is shown superimposed on the fascicle map, with the estimate marked by a *cross* and the true location by a *square*. (**d**) Localization results for all fascicles (single trial at 40% noise). The fascicle map is shown in *gray*, with true source locations as *red squares*, and a *green circle* centered on the estimated location. 10 trials, each 100 ms, were performed for each of the 10 fascicles modeled. The accuracy for the 40% noise trials, as pictured here, was 0.18 ± 0.17 mm ($N = 100$). Figure reproduced from Wodlinger and Durand [67] with permission from IEEE-TNSRE
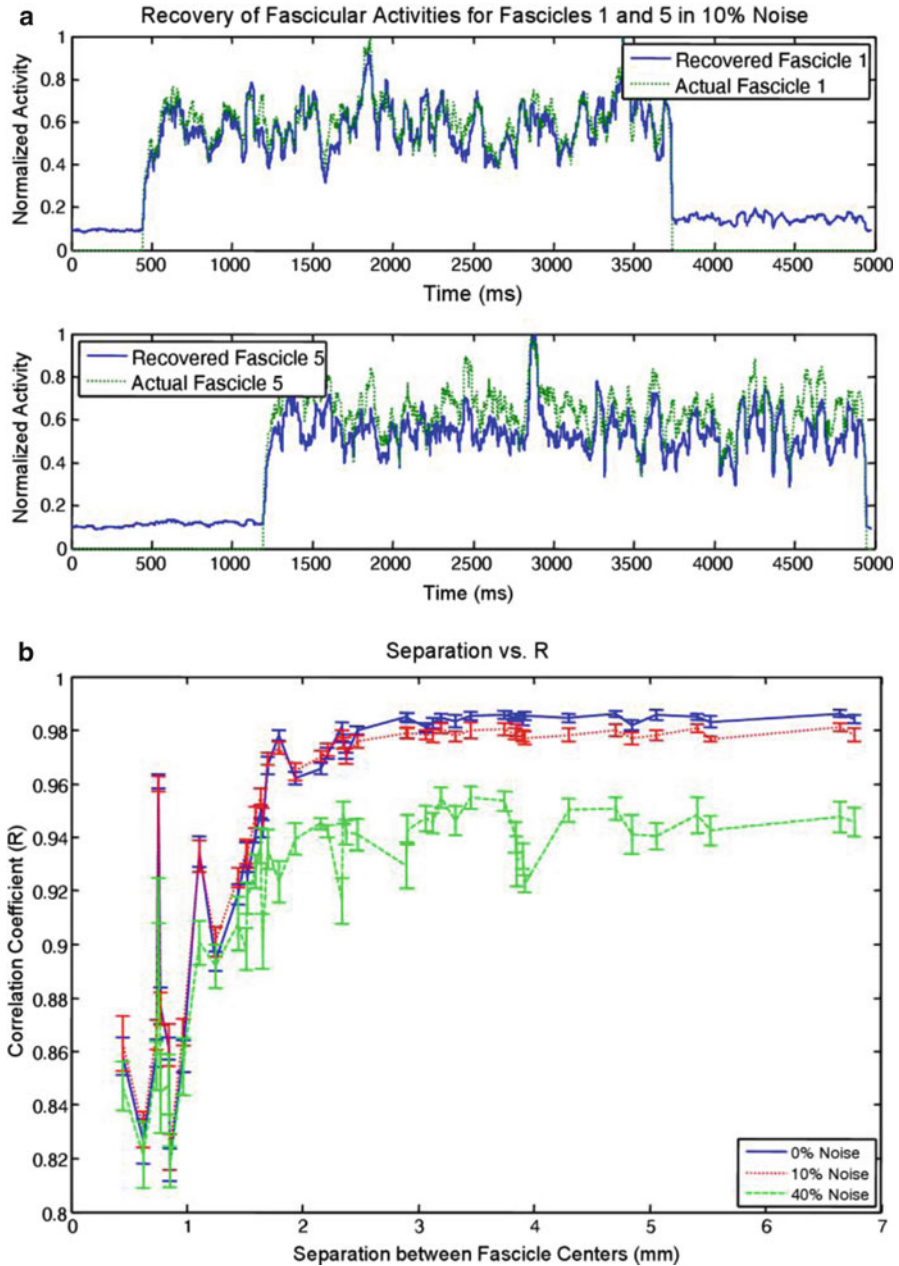
Fig. 16.4 Separating signals from pairs of simultaneous active fascicles. (**a**) Example recovered signal when fascicles 1 and 5 are active, including the actual activity level for each fascicle. Fascicles 1 and 5 are 5.5 mm apart and this trial resulted in $R = 0.97$. (**b**) Correlation coefficients and standard deviations for each fascicular separation distance at three noise levels. Ten trials were performed for each noise level and each trial included every possible pair of fascicles. Recovery

for *n* from 1 to 10, assuming the true source locations were known. For up to five simultaneously active fascicles, the reconstruction accuracy is unchanged with a mean value of $R = 0.74 \pm 0.18$ ($N = 50$). The accuracy decreases steadily as the number of active fascicles grows larger than five, reaching 80% of the single fascicle value for 10 simultaneously active fascicles. Recording noise has a strong effect on the reconstruction, lowering the mean value of the $n = 1 \ldots 5$ trials to $R = 0.61 \pm 0.18$ ($N = 50$), and dropping to 65% of the noisy single fascicle value for 10 simultaneously active fascicles.

2.6   Recovery of Neural Signals from a Rabbit Sciatic Nerve

The beamforming algorithm with Source-Based Filter (SBF) post-processing is demonstrated in a Rabbit sciatic nerve model. The high-density FINE was placed on the main trunk of the sciatic nerve near the popliteal fossa, while smaller stimulating cuff electrodes were placed on the two main branches, the tibial and peroneal. These smaller cuffs were stimulated with pulses to elicit compound action potentials which could be used to localize the activity from the two fascicle groups originating in the two branches. Sinusoidal stimulation was also delivered to create more realistic patterns of activity. This sinusoidal stimulation has the added benefit that any stimulation artifact can be easily removed from the recordings using filtering. This is not the case for traditional pulse stimulation due to the large number of harmonics created. Low-frequency sinusoids were found to elicit CAP-like discharges in phase with the sinusoid, while high-frequency stimulation produced pseudo-random activity, as described in Rubinstein et al. [78].

2.6.1   Recovery of Low-Frequency Evoked Activity

In order to test the ability of the algorithm to recover signals from the high-SNR low-frequency evoked activity, the Tibial and Peroneal fascicles were stimulated with a 130 Hz sinusoidal stimulus independently and recorded signals were then normalized and mixed off-line. Due to the linearity of the volume conductor, no generality is lost with the off-line mixing and it provides convenient single-source references for evaluating the separation quality. The stimulus artifact was removed and the beamforming filter matrix was applied to localize the activity within the nerve. An example of the recovered signals from the two identified sources is shown in Fig. 16.5. Filters for the two fascicle groups were calculated using the

---

Fig. 16.4 (continued) with negligible cross-talk is seen at $R = 0.9$, which for 10% noise occurs at approximately 1.5 mm—half the height of the cuff, and about twice the average fascicular diameter. Figure reproduced from Wodlinger and Durand [67] with permission from IEEE-TNSRE
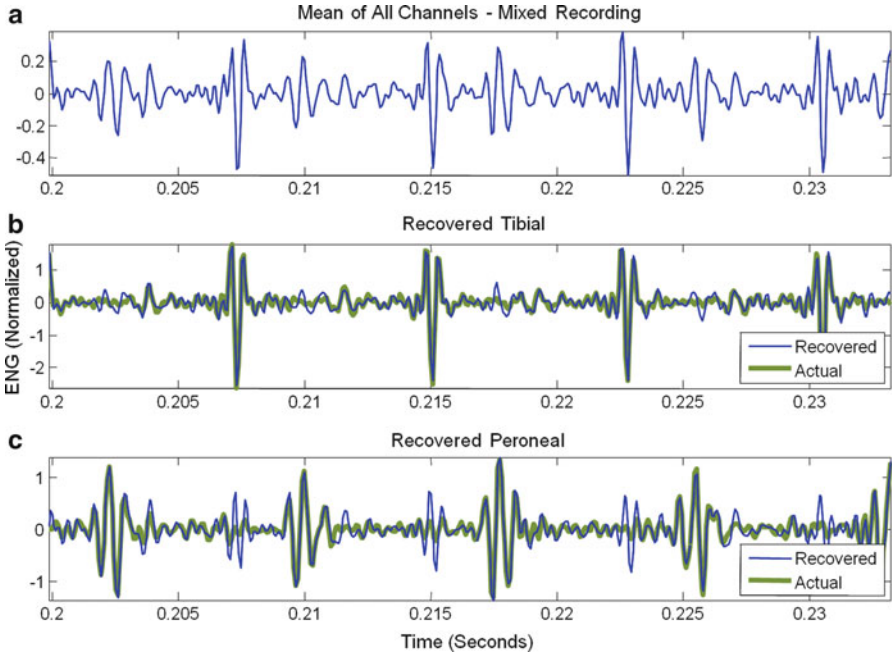
Fig. 16.5 Separation of Peroneal and Tibial components from combined signal using Beamforming filters. (**a**) The mean of all 16 channels (for clarity) for a signal created by adding a normalized recording during tibial stimulation with a normalized recording during peroneal stimulation. The beamformers were applied to this signal to generate an estimate for each branch, shown in (**b**) and (**c**) (Recovered signal). The two signals can easily be distinguished based on the shape of the responses, and the separation is nearly complete. The equivalent single-branch signals (calculated by applying the filters to the single-branch recordings directly) are shown as a *thick line* for reference [67] with permission from IEEE-TNSRE

SBF beamforming algorithm were then applied to the data. An example of the recovered signals from the two identified sources is shown in Fig. 16.5b, c. The correlation between the recovered and original signals was $R^2 = 0.81 \pm 0.08$ ($n = 14$). This represents an improvement of $30 \pm 14\%$ over simply using the best single channels in the mixed recording and $22 \pm 11\%$ over the beamforming filter matrix without any post-processing.

2.6.2 Effect of Contact Density and Position on Signal Recovery

The beamforming algorithm is a spatial filter, and so may be sensitive to the density of recording contacts on the electrode. In order to determine the role of contact density, the above experiments were repeated with 8 instead of 16 contacts. The above experiments were repeated offline recalculating the beamforming filter matrix using only half of the electrodes in the cuff. The R^2 value was reduced from
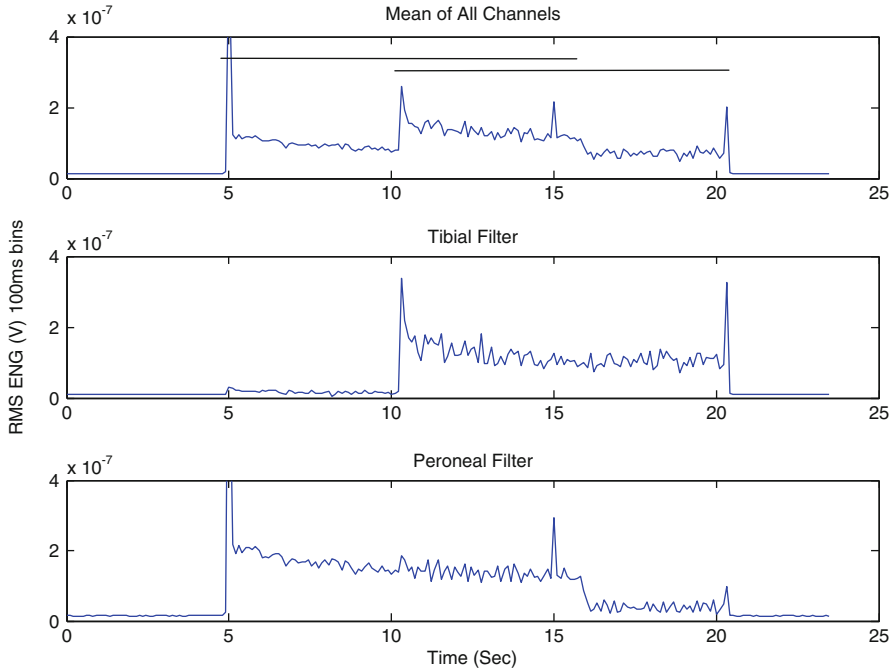
Fig. 16.6 Overlapping stimulation of the Peroneal and Tibial branches. (*Top*) The mean of all 16 channels in the rectified, integrated recording. *Black bars* indicate stimulation periods for the Peroneal (*left*) and Tibial (*right*) branches. (*Middle*) Output after applying Tibial beamforming filter to the rectified, integrated signal. (*Bottom*) Output after applying peroneal beamforming filter to the rectified, integrated signal. The cross talk between the two branches was $23 \pm 13\%$ ($N = 10$)

0.81 ± 0.08 to 0.47 ± 0.28 ($n = 14$) when only the top half of the electrode was used and to 0.59 ± 0.19 when only the evenly numbered contacts were used. This dramatic difference suggests that a high (2 contacts/mm) density of electrodes is required to achieve adequate performance.

2.6.3   Recovery of Pseudo-spontaneous Signals

High-frequency sinusoids were used to elicit pseudo-random activity in both fascicle groups in overlapping time windows. This test was repeated on five separate nerves and one typical example is shown in Fig. 16.6. The upper frame shows the mean of all 16 channels in the rectified and 100 ms bin-integrated recording. The mean of the 16 channels is used for clarity, since the 16 raw channels are difficult to visualize. The lower two frames show the outputs of the beamforming filter matrix with SBF post-processing acting on the rectified, 100 ms bin-integrated recording. The black bars in the upper frame correspond to

the stimulation intervals, with the peroneal branch stimulated first. The cross-talk between the two branches was $23 \pm 13\%$, calculated using periods when only one of the two branches was active, on 10 signals from 5 nerves. Without a reference for comparison uncontaminated by the overlapping activity, the accuracy of the separation cannot be calculated outside the windows where only one source was active.

Many techniques have been proposed to separate individual fascicular signals from whole peripheral nerve recordings, including Inverse Problem techniques, BSS, and Beamforming. While Inverse Problem techniques rely heavily on the accuracy of the system model, Blind source techniques do not assume any particular model, requiring only linear mixing of the statistically independent source signals. Beamforming represents a compromise, making use of some of the available model. A beamforming algorithm was investigated, along with a Source-based Filter post-processing, on both artificial and real neural recordings and demonstrated to provide $R^2 = 0.81 \pm 0.08$ separation of signals from two independent fascicular groups.

The ability to recover neural signals is only the first step in the larger goal of a closed loop system for neural control. A major component is the ability to control neural function with multiple contact nerve peripheral nerve electrodes. The following section describes in silico and in vivo experiments to study the ability of the FINE cuff to control the ankle joint.

3 Control of Multifasciculated Nerves with Selective Stimulation

A common strategy for system control is to first obtain an analytical model of the plant. Since it is very difficult to find accurate models of neuromuscular skeletal systems including the fascicular distribution inside a nerve trunk and the mapping from each fascicle to the target muscle(s) it innervates, we developed a new control method that does not require analytical modeling of the neuromuscular skeletal system. The controller finds an inverse dynamics of the system for control purposes using only measurable input and output data.

3.1 Controller Design

The controller is composed of an inverse steady state controller (ISSC), a feedforward controller, and a feedback controller as shown in Fig. 16.7. ISSC is an inverse model of the system at steady state. Feedforward controller is a dynamic inverse model of the combination of the system ISSC in series, and it is implemented with artificial neural networks. PID controller is used for feedback controller to compensate for external disturbances and system parameter variation.
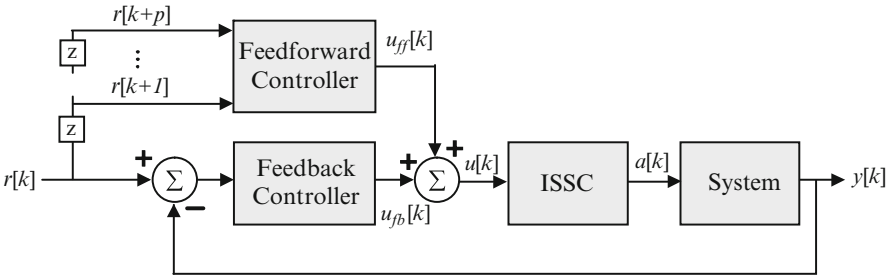
Fig. 16.7 The controller is composed of Inverse Steady State Controller (ISSC), Artificial Neural Network (ANN) feedforward controller, and PID feedback controller. $r[k]$ is the desired output, $y[k]$ is the system output, $u[k]$ is the input to ISSC, $o_{ff}[k]$ is the feedforward controller output, $o_f[k]$ is the feedback controller output, and $a[k]$ is the input to the system at time step k

3.2   Controller with Separated Static and Dynamic Properties

One of the difficulties in controlling the neuromuscular skeletal system can be attributed to the redundancy of the system. Due to this redundancy, an inverse model of the system is not uniquely determined and thus the direct inverse modeling approach has its limitation in obtaining a proper inverse model [79]. Therefore, we adopted a design that can reduce the redundancy by separating the static from the dynamic properties and can find the inverse model sequentially. The ISSC is obtained first with repetitive interpolation and extrapolation of existing steady-state data in the output joint coordinate. Once the ISSC is obtained, the feedforward controller is trained to learn the inverse dynamics of the combination of the ISSC and the system in series, whose redundancy has been drastically reduced.

In order to determine the performance of the controller, simulations were first carried out. A two-degree-of-freedom ankle-subtalar joint model with eight muscles was combined with the controller algorithm and the joint angles generated by the controller were compared to the desired angles. The simulation results show that the controller could generate small output tracking errors for various reference trajectories such as pseudo-step, sinusoidal, and filtered random signals. The results also indicate that the separation of the steady-state properties from the dynamics could minimize the problem of redundancy for the control of multiple input and multiple output (MIMO) systems [80]. The controller was then tested experimentally in rabbits and applied to the dynamic control of the ankle joint.

3.3   Multi-contact Electrode Control of Rabbit Ankle Joint

Animals were initially anesthetized with the injection of ketamine (50 mg/kg) and xylazine (5 mg/kg), and then maintained with 1–3% isoflurane mixed with pure oxygen or medical gas. A surgical incision was made on the posterior thigh to

expose the sciatic nerve around the branching point to common peroneal nerve and tibial nerve. Then a 14-contact FINE with seven contacts on each side was implanted on the sciatic nerve proximal to the branching point. After suturing closed the incision, the rabbit was placed on the measurement instrument in the prone position. The foot was secured to the armature, and the knee joint was maintained at approximately 90°. A needle electrode was inserted under the skin of the contralateral hip as a returning electrode.

The performance of the rabbit ankle joint motion control was tested for sinusoidal reference trajectories and filtered random trajectories. An example of the control performance is shown in Fig. 16.8. The normalized RMS errors for sinusoidal signals with 0.5 Hz and 1.0 Hz for a total of eight legs were $7.2 \pm 1.6\%$ and $9.9 \pm 1.9\%$, respectively. Although the RMS error for higher frequency is greater than lower frequency ($p < 0.05$), the time delay between the desired trajectories and the measured trajectories was negligible in both cases. The normalized RMS error for low pass filtered random trajectories with cutoff frequency of 1.0 Hz was $6.0 \pm 1.0\%$. The control system was then applied to the more complex human ankle joint motion.

3.4 In Silico Control of Human Ankle

A computation model of a human ankle joint system with the sciatic nerve was developed for the simulation study. The ankle-subtalar joint model has 12 muscles and 2 hinge joints, which was adopted from the lower extremity model [81]. The 12 muscles in this model are medial gastrocnemius (MG), lateral gastrocnemius (LG), soleus (Sol), tibialis anterior (TA), tibialis posterior (TP), peroneus brevis (PB), peroneus longus (PL), peroneus tertius (PT), extensor digitorum longus (EDL), extensor hallucis longus (EHL), flexer digitorum longus (FDL), and flexor hallucis longus (FHL). Musculographics SIMM and SD/FAST were used for the modeling and simulation of musculoskeletal system [82]. The inputs to the musculoskeletal model were the muscle excitation level of each muscle between 0 (no excitation) and 1 (maximum excitation), and the outputs were the ankle and subtalar joint angles. The range of motion of the ankle joint and subtalar joint was −40° to 20° and −20° to 20°, respectively.

The nervous system model was based on histological data of human sciatic nerve. A FINE was hypothetically placed on the sciatic nerve proximal to the branching point to the common peroneal and tibial nerves so that a single FINE could control both dorsiflexion/planter flexion and inversion/eversion. Since the mapping from the fascicles to the target muscles was unknown, we arbitrarily assigned the mapping according to maximum muscle strength and geometrical proximity of each fascicle to tibial or common peroneal branches. After the fascicular redistribution was determined by the reshaping algorithm, we used finite element method to find voltage distribution inside the fascicles with Ansoft Maxwell. The conductivity of endoneurium, epineurium, and perineurium in the
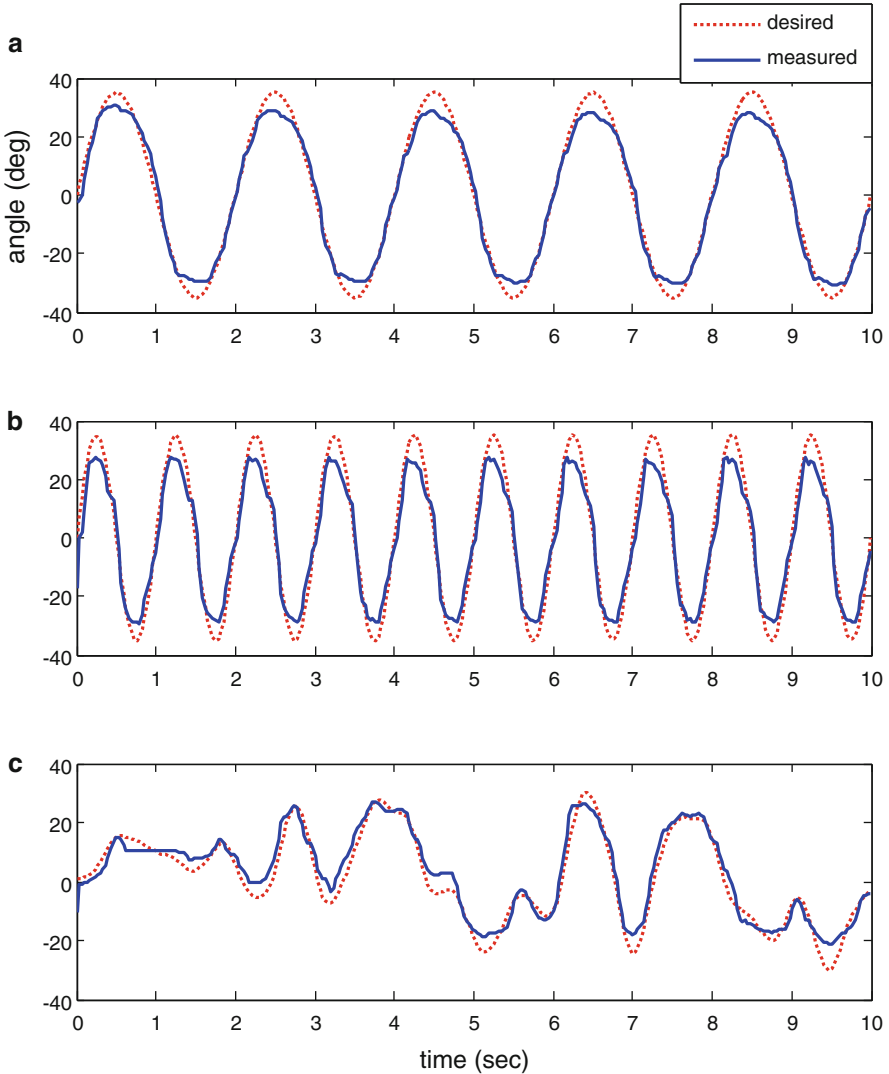
Fig. 16.8 Results for (**a**) sinusoidal trajectory with 0.5 Hz (RMS error: 3.5°), (**b**) sinusoidal trajectory with 1.0 Hz (RMS error: 5.6°), (**c**) filtered random trajectory (RMS error: 3.6°)

neuronal model is shown in Table 16.1. The axons inside the fascicles are located uniformly with 50 μm distance between the two adjacent axons in transversal plane. The axonal diameter has Gaussian distribution between 10 μm and 20 μm, and a single layer cable model was adopted for axon model [60]. The axon model has 15 nodes and we used NEURON to run simulations with a cathodic pulse with pulse width of 50 μs. We assumed that adjacent contacts are sequentially stimulated within the refractory period. We also assumed that the muscle excitation level is the

Table 16.1 Parameters used in FEM simulations

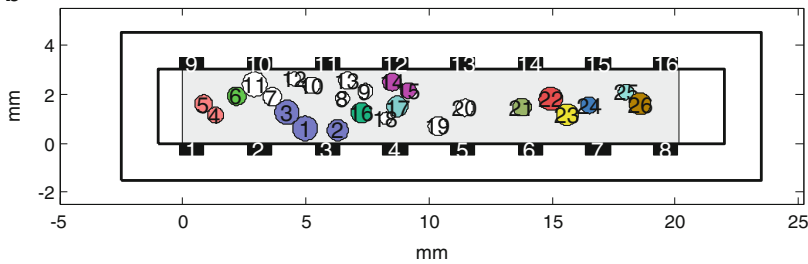| Material	Conductivity (S/m) [43]	Parameter	Length (mm)
Epineurium	0.083	Cuff height	3
Saline	2.000	Cuff length	15
Endoneurium (trans.)	0.083	Cuff width	12
Endoneurium (long.)	0.571	Saline volume	$150 \times 200 \times 150$
Perineurium	0.002		
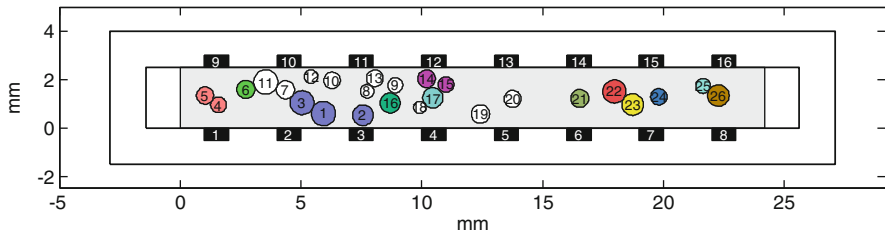
Fig. 16.9 Each fascicle in the sciatic nerve is modeled as a regular dodecagon. The fascicles are mapped to the muscles as follows: 1,2,3: Sol, 4,5: MG, 6: LG, 14,15: TP, 16: FHL, 17: FDL, 21: EHL, 22: EDL, 23: TA, 24: PT, 25: PB, 26: PL. (**a**) Realignment of fascicles with a FINE of 2.5 mm height. (**b**) Realignment of fascicles with a FINE of 3.0 mm height

weighted sum of excited axons over the total axons proportional to the axonal cross-sectional area.

For each of two different configurations with cuff heights of 2.5 mm and 3.0 mm shown in Fig. 16.9, three different controllers were tried with different combinations of contacts selected. The average RMS errors for sinusoidal reference trajectories between 0.5 Hz and 1.0 Hz with random amplitudes and random phase difference between ankle and subtalar joint angles were $1.6 \pm 1.1°$ for ankle joint and $1.6 \pm 0.7°$ for subtalar joint, which are less than 5% of the maximum range of the motion. In order to show the robustness of the controller, the maximum strength of each muscle was randomly decreased up to 50%. For filtered random reference

trajectories, the average RMS errors were $1.6 \pm 0.5°$ for ankle and $1.4 \pm 0.3°$ for subtalar joint, which are only a little increased from the simulation without muscle fatigue ($1.4 \pm 1.1°$, $1.2 \pm 0.3°$). In addition, a time varying external force was applied to the foot with the maximum strength of 25 N to show the robustness of the controller against external disturbance. The output error for sinusoidal reference signals increased to $2.1 \pm 1.2°$ and $1.7 \pm 0.7°$ from $1.6 \pm 1.1°$ and $1.6 \pm 0.7°$ for ankle and subtalar joint angle, respectively. However, even with the time varying external disturbance, the average output angle errors were within 5% of the maximum range of motion. These results show that a motion controller using a FINE could be built without analytical modeling.

4   Conclusions

Significant research in the design of effective and functional interfaces has been carried in the last few years with the central nervous system interfaces known as brain machine interfaces (BMI) leading the way particularly in the clinical area. However, progress has also been made in interfacing with the peripheral nervous system. Several electrode designs either penetrating the fascicles or external to the nerve (cuff) have been proposed, each with their advantages and disadvantages and it is not clear at this time which design will be most successful.

In this chapter, we have concentrated on the results obtained with the flat cuff electrode design (FINE) and for this type of electrode, several conclusions can be made:

- The flat interface nerve electrode presents a unique opportunity to place a large number of electrodes on the circumference of a nerve safely.
- Fascicular sources within the cross section of a peripheral can be imaged.
- Fascicular signals can be recovered selectively using beamforming algorithms as demonstrated both in silico and in vivo animal experiments.
- The challenge of controlling a neuromuscular skeletal dynamic system with multiple contact nerve electrodes can be met.
- Separation of the static and dynamic properties of the system to be controlled can reduce the problem of redundancy inherent to most multiple input multiple output systems (MINO) such as the ankle joint.

Taken together these results suggest that it might soon be possible to obtain neural signals from the peripheral nerve and provide amputees with a neurotechnology-based solution for the voluntary control of an artificial limb. Moreover, the combination of the neural recording and neural control presented above would also provide a closed loop neural control of neural function.

References

1. Lundborg G (1988) The nerve trunk. In: Nerve injury and repair. Chruchill Livingstone, Edinburgh, Scotland, pp 36–42
2. Slot PJ, Selmar P et al (1997) Effect of long-term implanted nerve cuff electrodes on the electrophysiological properties of human sensory nerves. Artif Organs 21(3):207–209
3. Cavanaugh JK, Lin JC et al. (1996) Finite element analysis of electrical nerve stimulation. Engineering in Medicine and Biology Society. Bridging Disciplines for Biomedicine. In: Proceedings of the 18th Annual International Conference of the IEEE 1:355–356
4. Altman KW, Plonsey R (1990) Point source nerve bundle stimulation: effects of fiber diameter and depth on simulated excitation. IEEE Trans Biomed Eng 37(7):688–698
5. Veltink PH, Van Alste JA et al (1988) Influences of stimulation conditions on recruitment of myelinated nerve fibers: a model study. IEEE Trans Biomed Eng 35(11):917–924
6. Veltink PH, van Alste JA et al (1989) Multielectrode intrafascicular and extraneural stimulation. Med Biol Eng Comput 27(1):19–24
7. Grill WM Jr, Mortimer JT (1996) The effect of stimulus pulse duration on selectivity of neural stimulation. IEEE Trans Biomed Eng 43(2):161–166
8. Grill WM Jr, Mortimer JT (1996) Quantification of recruitment properties of multiple contact cuff electrodes. IEEE Trans Rehabil Eng 4(2):49–62
9. Deurloo KEI, Boere CJP et al (1997) Optimization of inactivating current waveform for selective peripheral nerve stimulation. In: Proceedings of the second annual IFESS conference and neural prosthesis: motor systems 5, Burnaby, BC, Canada
10. Goodall EV, de Breij JF et al (1996) Position-selective activation of peripheral nerve fibers with a cuff electrode. IEEE Trans Biomed Eng 43(8):851–856
11. Naples GG, Mortimer JT et al (1988) A spiral nerve cuff electrode for peripheral nerve stimulation. IEEE Trans Biomed Eng 35(11):905–916
12. Rozman J, Trlep M (1992) Multielectrode spiral cuff for selective stimulation of nerve fibres. J Med Eng Technol 16(5):194–203
13. Rodriguez FJ, Ceballos D et al (2000) Polyimide cuff electrodes for peripheral nerve stimulation. J Neurosci Methods 98(2):105–118
14. Navarro X, Valderrama E et al (2001) Selective fascicular stimulation of the rat sciatic nerve with multipolar polyimide cuff electrodes. Restor Neurol Neurosci 18(1):9–21
15. Agnew WF, McCreery DB (1990) Considerations for safety with chronically implanted nerve electrodes. Epilepsia 31(Suppl 2):S27–S32
16. Hansen M, Haugland MK et al (2004) Evaluating robustness of gait event detection based on machine learning and natural sensors. IEEE Trans Neural Syst Rehabil Eng 12(1):81–88
17. Hoffer JA, Stein RB et al (1996) Neural signals for command control and feedback in functional neuromuscular stimulation: a review. J Rehabil Res Dev 33(2):145–157
18. Sahin M, Haxhiu MA et al (1997) Spiral nerve cuff electrode for recordings of respiratory output. J Appl Physiol 83(1):317–322
19. Struijk JJ, Haugland MK, Thomsen M (1996) Fascicle selective recording with a nerve cuff electrode. In: Proceedings of the 18th annual international IEEE/EMBS conference, Amsterdam, The Netherlands
20. Christensen PR, Chen Y, Strange KD, Yoshida K, Hoffer JA (1997) Multi-channel recordings from peripheral nerves: 4. Evaluation of selectivity using mechanical stimulation of individual digits. In: Proceedings of the second annual IFESS conference and neural prosthesis: Motor systems 5. Burnaby, BC, Canada
21. Rozman J, Zorko B et al (2000) Selective recording of electroneurograms from the sciatic nerve of a dog with multi-electrode spiral cuffs. Jpn J Physiol 50(5):509–514
22. Rozman J, Zorko B et al (2000) Selective recording of neuroelectric activity from the peripheral nerve. Pflugers Arch 440(5 Suppl):R157–R159

23. Kovacs GT, Storment CW et al (1994) Silicon-substrate microelectrode arrays for parallel recording of neural activity in peripheral and cranial nerves. IEEE Trans Biomed Eng 41(6):567–577
24. Akin T, Najafi K et al (1994) A micromachined silicon sieve electrode for nerve regeneration applications. IEEE Trans Biomed Eng 41(4):305–313
25. Shimatani Y, Nikles SA et al (2003) Long-term recordings from afferent taste fibers. Physiol Behav 80(2–3):309–315
26. Rutten WL, Frieswijk TA et al (1995) 3D neuro-electronic interface devices for neuromuscular control: design studies and realisation steps. Biosens Bioelectron 10(1–2):141–153
27. Branner A, Stein RB et al (2001) Selective stimulation of cat sciatic nerve using an array of varying-length microelectrodes. J Neurophysiol 85(4):1585–1594
28. Branner A et al (2001) Selective stimulation of cat sciatic nerve using an array of varying-length microelectrodes. J Neurophysiol 85:1585
29. Goodall EV, Horch KW et al (1993) Analysis of single-unit firing patterns in multi-unit intrafascicular recordings. Med Biol Eng Comput 31(3):257–267
30. Smit JP, Rutten WL et al (1999) Endoneural selective stimulating using wire-microelectrode arrays. IEEE Trans Rehabil Eng 7(4):399–412
31. Djilas M, Azevedo-Coste C et al (2009) Interpretation of muscle spindle afferent nerve response to passive muscle stretch recorded with thin-film longitudinal intrafascicular electrodes. IEEE Trans Neural Syst Rehabil Eng 17(5):445–453
32. Djilas M, Azevedo-Coste C et al (2010) Spike sorting of muscle spindle afferent nerve activity recorded with thin-film intrafascicular electrodes. Comput Intell Neurosci. doi:10.1155/2010/836346
33. Yoshida K, Horch K (1993) Reduced fatigue in electrically stimulated muscle using dual channel intrafascicular electrodes with interleaved stimulation. Ann Biomed Eng 21(6):709–714
34. Micera S, Navarro X et al (2008) On the use of longitudinal intrafascicular peripheral interfaces for the control of cybernetic hand prostheses in amputees. IEEE Trans Neural Syst Rehabil Eng 16(5):453–472
35. Rossini PM, Micera S et al (2010) Double nerve intraneural interface implant on a human amputee for robotic hand control. Clin Neurophysiol 121(5):777–783
36. Bowman BR, Erickson RC 2nd (1985) Acute and chronic implantation of coiled wire intraneural electrodes during cyclical electrical stimulation. Ann Biomed Eng 13(1):75–93
37. Boretius T, Badia J et al (2010) A transverse intrafascicular multichannel electrode (TIME) to interface with the peripheral nerve. Biosens Bioelectron 26(1):62–69
38. Tyler DJ, Durand DM (2002) Functionally selective peripheral nerve stimulation with a flat interface nerve electrode. IEEE Trans Neural Syst Rehabil Eng 10(4):294–303
39. Gustafsan KJ, Neville J et al (2003) Fascicular anatomy of the human femoral nerve: implication for standing neural prostheses utilizing nerve cuff electrodes. In: 34th Annual NIH neural prosthesis workshop, Bethesda, MD, USA
40. Larsen JO, Thomsen M et al (1998) Degeneration and regeneration in rabbit peripheral nerve with long-term nerve cuff electrode implant: a stereological study of myelinated and unmyelinated axons. Acta Neuropathol (Berl) 96(4):365–378
41. Sweeney JD, Ksienski DA et al (1990) A nerve cuff technique for selective excitation of peripheral nerve trunk regions. IEEE Trans Biomed Eng 37(7):706–715
42. Agnew WF, McCreery DB et al (1989) Histologic and physiologic evaluation of electrically stimulated peripheral nerve: considerations for the selection of parameters. Ann Biomed Eng 17(1):39–60
43. Choi AQ, Cavanaugh JK et al (2001) Selectivity of multiple-contact nerve cuff electrodes: a simulation analysis. IEEE Trans Biomed Eng 48(2):165–172
44. Leventhal DK, Durand DM (2003) Subfascicle stimulation selectivity with the flat interface nerve electrode. Ann Biomed Eng 31(6):643–652

45. Tyler DJ, Durand DM (2003) Chronic response of the rat sciatic nerve to the flat interface nerve electrode. Ann Biomed Eng 31(6):633–642
46. Schiefer MA, Polasek KH et al (2010) Selective stimulation of the human femoral nerve with a flat interface nerve electrode. J Neural Eng 7(2):26006
47. Tasaki I (1953) Nervous transmission. Charles C Thomas, Springfield, IL
48. Henneman E, Somjen G et al (1965) Functional significance of cell size in spinal motoneurons. J Neurophysiol 28:560–580
49. Solomonow M (1984) External control of the neuromuscular system. IEEE Trans Biomed Eng 31(12):752–763
50. Koldewijn EL, Rijkhoff NJ et al (1994) Selective sacral root stimulation for bladder control: acute experiments in an animal model. J Urol 151(6):1674–1679
51. Rijkhoff NJ, Wijkstra H et al (1997) Selective detrusor activation by electrical sacral nerve root stimulation in spinal cord injury. J Urol 157(4):1504–1508
52. Bhadra N, Grunewald V et al (2002) Selective suppression of sphincter activation during sacral anterior nerve root stimulation. Neurourol Urodyn 21(1):55–64
53. Fang ZP, Mortimer JT (1991) A method to effect physiological recruitment order in electrically activated muscle. IEEE Trans Biomed Eng 38(2):175–179
54. Rozman J, Sovinec B et al (1993) Multielectrode spiral cuff for ordered and reversed activation of nerve fibres. J Biomed Eng 15(2):113–120
55. Tai C, Jiang D (1994) Selective stimulation of smaller fibers in a compound nerve trunk with single cathode by rectangular current pulses. IEEE Trans Biomed Eng 41(3):286–291
56. Grill WM and Mortimer JT, Stimulus waveforms for selective neural stimulation (1995) Engineering in Medicine and Biology Magazine, IEEE 14:375–385
57. Van Bolhuis AI, Holsheimer J et al (2001) A nerve stimulation method to selectively recruit smaller motor-units in rat skeletal muscle. J Neurosci Methods 107(1–2):87–92
58. Deurloo KE, Holsheimer J et al (2001) The effect of subthreshold prepulses on the recruitment order in a nerve trunk analyzed in a simple and a realistic volume conductor model. Biol Cybern 85(4):281–291
59. Robblee LS, Rose TL (1990) Electrochemical guidelines for selection of protocols and electrode materials for neural stimulation. In: Agnew WF, McCreery DB (eds) Neural prosthesis: fundamental studies. Prentice Hall, Englewood Cliffs, NJ
60. Lertmanorat Z, Durand DM (2004) A novel electrode array for diameter-dependent control of axonal excitability: a simulation study. IEEE Trans Biomed Eng 51(7):1242–1250
61. Lertmanorat Z, Durand DM (2003) Reversing the recruitment order with electrode array stimulation. In: Proceedings of the 25th international conference of the IEEE/EMBS, Cancun, Mexico
62. Loeb GE, Peck RA (1996) Cuff electrodes for chronic stimulation and recording of peripheral nerve activity. J Neurosci Methods 64(1):95–103
63. Leventhal DK, Cohen M et al (2006) Chronic histological effects of the flat interface nerve electrode. J Neural Eng 3(2):102–113
64. Wolpaw JR, McFarland DJ (2004) Control of a two-dimensional movement signal by a noninvasive brain-computer interface in humans. Proc Natl Acad Sci USA 101(51):17849–17854
65. Zariffa J, Popovic MR (2008) Application of EEG source localization algorithms to the monitoring of active pathways in peripheral nerves. In: 30th Annual international IEEE EMBS conference, Vancouver, BC, Canada
66. Tesfayesus W, Durand DM (2007) Blind source separation of peripheral nerve recordings. J Neural Eng 4(3):S157–S167
67. Wodlinger B, Durand DM (2009) Localization and recovery of peripheral neural sources with beamforming algorithms. IEEE Trans Neural Syst Rehabil Eng 17(5):461–468
68. Calvetti D, Hakula H et al (2009) Conditionally Gaussian hypermodels for cerebral source localization. SIAM J Imag Sci 2(3)

69. Nissinen A, Heikkinen LM et al (2008) The Bayesian approximation error approach for electrical impedance tomography—experimental results. Meas Sci Technol 19(1):015501
70. Michel C, He B (eds) (2011) EEG mapping and source imaging. In: Niedermeyer's electroencephalography. Wolters Kluwer & Lippincott Williams & Wilkins, Philadelphia
71. Sekihara K, Nagarajan SS (2008) Adaptive spatial filters for electromagnetic brain imaging. Springer, New York
72. Wodlinger B, Durand DM (2010) Peripheral nerve signal recording and processing for artificial limb control. Conf Proc IEEE Eng Med Biol Soc 2010:6206–6209
73. Schiefer MA, Triolo RJ et al (2008) A model of selective activation of the femoral nerve with a flat interface nerve electrode for a lower extremity neuroprosthesis. IEEE Trans Neural Syst Rehabil Eng 16(2):195–204
74. Otsu N (1979) A threshold selection method from gray-level histograms. IEEE Trans Syst Man Cybern 9(1):62–66
75. Jezernik S, Sinkjaer T (1999) On statistical properties of whole nerve cuff recordings. IEEE Trans Biomed Eng 46(10):1240–1245
76. Yoo PB, Durand DM (2005) Selective recording of the canine hypoglossal nerve using a multicontact flat interface nerve electrode. IEEE Trans Biomed Eng 52(8):1461–1469
77. Tesfayesus W, Yoo P, Moffitt M, Durand DM (2003) Blind source separation of nerve cuff recordings. In: Proceedings of the 25th international conference of the IEEE/EMBS, Cancun, Mexico
78. Rubinstein JT, Wilson BS et al (1999) Pseudospontaneous activity: stochastic independence of auditory nerve fibers with electrical stimulation. Hear Res 127(1–2):108–118
79. Jordan MI, Rumelhart DE (1992) Forward models—supervised learning with a distal teacher. Cogn Sci 16(3):307–354
80. Park H, Durand D (2008) Motion control of musculoskeletal systems with redundancy. Biol Cybern 99(6):503–516
81. Heilman B, Audu M et al (2006) Selection of an optimal muscle set for a 16-channel standing neuroprosthesis using a human musculoskeletal model. J Rehabil Res Dev 43(2):273–286
82. Delp SL (1990) Surgical simulation : a computer graphics system to analyze and design musculoskeletal reconstructions of the lower limb. Ph.D. Dissertation, Stanford